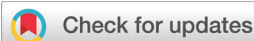


## RESEARCH ARTICLE

[View Article Online](#)  
[View Journal](#) | [View Issue](#)

 Cite this: *Inorg. Chem. Front.*, 2023, **10**, 2430

# Achieving efficient violet-light-excited blue phosphors by nitridation for violet-chip-based full-spectrum lighting†

 Chao Dou, Fangyi Zhao, Shengqiang Liu, Zhen Song  and Quanlin Liu \*

With the pursuit of healthy lighting, full-spectrum white light-emitting diodes (WLEDs) fabricated with violet chips and tri-color phosphors have been put forward. However, the excitation bands of most reported blue phosphors are located in the ultraviolet (UV) region, which hinders the development of full-spectrum lighting. In this work, by partially introducing  $N^{3-}$  into a matrix, a series of  $Ba_{0.697}Al_{10.914}O_{17.232-3y/2}N_y:0.16Eu^{2+}$  ( $BAON_y:Eu$ ) blue phosphors with red-shifted photoluminescence excitation (PLE) spectra were synthesized. Under the excitation of 400 nm violet light, the internal/external quantum efficiency (IQE/EQE) values of the optimal sample  $BAON_{1.0}:Eu$  were calculated to be 80%/52%, while the retained integrated emission intensity at 150 °C can be 95% of that at room temperature. The WLED device fabricated by coating  $BAON_{1.0}:Eu$  and other commercial phosphors on a violet chip achieved an ultra-high color rendering index ( $R_a = 95.4$ ). These results indicate that our synthesized  $BAON_{1.0}:Eu$  can be an excellent candidate blue phosphor for full-spectrum WLED lighting.

Received 23rd November 2022,

Accepted 17th March 2023

DOI: 10.1039/d2qi02489f

[rsc.li/frontiers-inorganic](https://rsc.li/frontiers-inorganic)

## 1. Introduction

White light-emitting diodes (WLEDs), as the fourth generation lighting source, have the advantages of high efficiency, long lifetime, saving energy, *etc.*<sup>1,2</sup> Commercially, WLEDs are fabricated by combining blue GaN chips with commercial YAG:  $Ce^{3+}, Eu^{2+}$ -doped silicate and nitride phosphors, but the excess blue light is harmful to human eyes.<sup>3–6</sup> With the pursuit of high-quality, comfortable and healthy lighting, full-spectrum WLEDs have attracted great enthusiasm in the academic and commercial fields.<sup>7–9</sup> Full-spectrum WLEDs are generally fabricated by combining near ultraviolet (n-UV, 365–400 nm) or violet chips (400–420 nm) with various phosphors.<sup>10,11</sup> The WLEDs based on n-UV chips have the advantage of good spectral continuity without a gap.<sup>12,13</sup> However, human eyes feature low perception to UV light and UV light is harmful to the human body.<sup>14,15</sup> Compared with n-UV chips, violet chips can meet the requirements of full-spectrum WLED fabrication, and the external efficiency of violet chips is about 80%, higher than that of 365 nm n-UV chips (44%).<sup>16,17</sup> Therefore, WLEDs based on violet chips have important application prospects. This also puts forward higher requirements for the phosphors

that can be efficiently excited by violet light. Currently, many reported red and green phosphors have satisfied the above-mentioned requirements, but few blue phosphors can meet the packaging requirements due to low efficiency and bad thermal stability, and especially their mismatch with violet chips.<sup>18–23</sup>

The luminescence performance of the parity-allowed 4f–5d transition ( $Eu^{2+}$  and  $Ce^{3+}$  ions) is highly dependent on coordinated crystalline environments.<sup>24</sup> Cation substitution, cationic pair co-substitution, anion modification and second coordination layer regulation are all favorable to tune luminescence performances of phosphors.<sup>25,26</sup> For example, the substitution of Lu and Gd for Y in  $Y_3Al_5O_{12}:Ce$  can produce a series of green-yellow color-tunable phosphors, which can be attributed to the variation of the crystal field strength of  $Ce^{3+}$ .<sup>27</sup> Besides, by controlling the ratio of F and Cl in  $Rb_{0.5}K_{1.5}CaPO_4(F,Cl):Eu$ , white light-emission can be realized through regulating the lattice site occupancy of  $Eu^{2+}$  and assembling multi-color emissions in different crystal field environments.<sup>28</sup>

A highly symmetric and rigid  $\beta-Al_2O_3$  structure is an excellent matrix for  $Eu^{2+}$  doping. A series of  $Eu^{2+}$ -doped  $\beta-Al_2O_3$  blue phosphors with outstanding luminescence performance, such as  $BaMgAl_{10}O_{17}:Eu$ ,  $KAl_{11}O_{17}:Eu$  and  $Ba_{0.857}Al_{10.914}O_{17.232}:Eu$ , have been reported in recent years.<sup>29–32</sup> However, the poor absorption efficiency in the violet region obstructs their further applications. To solve the problem of mismatch with violet chips, it is significant to tune

The Beijing Municipal Key Laboratory of New Energy Materials and Technologies, School of Materials Science and Engineering, University of Science and Technology Beijing, Beijing 100083, China. E-mail: [qlliu@ustb.edu.cn](mailto:qlliu@ustb.edu.cn)

† Electronic supplementary information (ESI) available. See DOI: <https://doi.org/10.1039/d2qi02489f>

the excitation spectrum. In addition to cation substitution and cationic pair co-substitution, anion modification is an easy and skillful strategy to regulate the excitation spectrum because the type of coordination anion has a great influence on the 5d centroid shift.<sup>33,34</sup> Compared with oxides, nitrides with higher covalency usually have a low centroid position,<sup>35</sup> which is favorable to make the excitation spectrum red-shift. Herein, based on  $\text{Ba}_{0.857}\text{Al}_{10.914}\text{O}_{17.232}$  (BAO) with a  $\beta\text{-Al}_2\text{O}_3$  structure, an efficient and thermally stable blue  $\text{Ba}_{0.697}\text{Al}_{10.914}\text{O}_{15.732}\text{N}_{1.0}:0.16\text{Eu}^{2+}$  ( $\text{BAON}_{1.0}:\text{Eu}$ ) phosphor, which can be effectively excited by 400 nm violet light, was realized by partial substitution of  $\text{N}^{3-}$  for  $\text{O}^{2-}$ . A WLED device fabricated using a violet chip and  $\text{BAON}_{1.0}:\text{Eu}$  phosphor can generate a full-spectrum white light with an ultra-high color rendering index ( $R_a$ ), indicating that  $\text{BAON}_{1.0}:\text{Eu}$  can be a promising blue-emitting phosphor for full-spectrum lighting application.

## 2. Experimental section

### 2.1. Materials and synthetic procedures

$\text{BAON}_y:\text{Eu}$  ( $y = 0, 0.2, 0.4, 0.6, 0.8, 1.0$ ) samples were prepared by the conventional high-temperature solid state method (the doping concentration of  $\text{Eu}^{2+}$  in this work was chosen to be 16 at%, since an impurity phase will appear upon further increasing  $\text{Eu}^{2+}$  content in BAO.<sup>22</sup>). Raw materials of  $\text{BaCO}_3$  (99.9%),  $\text{Al}_2\text{O}_3$  (99.9%),  $\text{AlN}$  (99.9%) and  $\text{Eu}_2\text{O}_3$  (99.99%) were weighed according to the stoichiometric ratio, and 4 wt%  $\text{AlF}_3$  was also added as a flux. The raw materials were ground with ethanol in an agate mortar for more than 20 minutes. Then, the well-mixed raw materials were transferred to alumina crucibles and sintered at 1600 °C for 4.5 hours (in a tube furnace, BEQ BTF 1700C) under a reducing atmosphere (20%  $\text{H}_2$ , 80%  $\text{N}_2$ ). Finally, the well-sintered samples were naturally cooled to room temperature and ground into fine powders for subsequent characterization studies. A WLED device was packaged by combining a 405 nm violet chip with our synthesized  $\text{BAON}_{1.0}:\text{Eu}$  and other commercial  $(\text{Sr},\text{Ba})_2\text{SiO}_4:\text{Eu}$ ,  $\text{Sr}_3\text{SiO}_5:\text{Eu}$  and  $\text{CaAlSiN}_3:\text{Eu}$  phosphors. The weight ratio of  $\text{BAON}_{1.0}:\text{Eu} : (\text{Sr},\text{Ba})_2\text{SiO}_4:\text{Eu} : \text{Sr}_3\text{SiO}_5:\text{Eu} : \text{CaAlSiN}_3:\text{Eu}$  is 10 : 3 : 4 : 1.

During the fabrication process, high refracting glue and phosphors were mixed thoroughly with the aid of an ultrasonic machine for more than 10 minutes. Then, the mixture was dripped onto a violet chip and dried in a box oven at 60 °C for 40 minutes, and then kept at 135 °C for 120 minutes to solidify the WLED device.

### 2.2. Characterization

The X-ray diffraction (XRD) patterns of  $\text{BAON}_y:\text{Eu}$  were recorded on a diffractometer (TTR III, Rigaku, Japan) with  $\text{Cu K}\alpha 1$  radiation (40 kV, 200 mA,  $\lambda = 1.5406 \text{ \AA}$ ). The Fullprof program was used for Rietveld refinement (in the range of 5 to 120 degrees) and neutron diffraction (ND) pattern calculations. Morphology observation and energy-dispersive spectroscopy (EDS) elemental mapping were performed using a scanning electron microscope (SEM, JEOL JSM-6510, Japan). The N element content was measured using a RUIYAN ONH330 instrument. Photoluminescence (PL) and photoluminescence excitation (PLE) spectra were recorded using a fluorescence spectrophotometer (FLS920, Edinburgh Instruments), equipped with a 150 W Xe lamp as the steady-state excitation source. The temperature-dependent PL spectra were recorded using a fluorescence spectrophotometer equipped with an Oxford Instruments temperature variation platform. The internal/external quantum efficiency (IQE/EQE) values were measured using an absolute PL quantum yield spectrometer (Quantaury-QY Plus C13534-11, Hamamatsu Photonics). The electroluminescence (EL) spectra of the packaged WLED were recorded using a photoelectric measuring system (LHS-1000, EVERFINE) equipped with a spectrophotometer (350–1100 nm, HAAS-2000).

## 3. Results and discussion

### 3.1. Crystal structure and XRD analysis

Fig. 1 shows the crystal structure of hexagonal BAO with a  $P6_3/mmc$  space group; the corresponding atomic coordinates and occupancy are listed in Table S1.<sup>†</sup><sup>36</sup> This structure consists of two kinds of Ba (Ba1 and Ba2), five kinds of Al (Al1–Al5) and

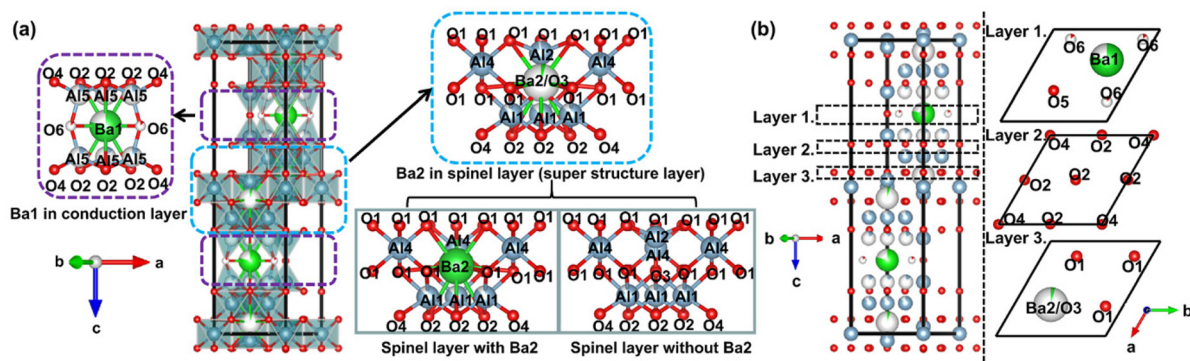


**Fig. 1** (a) Conduction layer and spinel layer of the BAO structure as well as the coordination environment of Ba1 and Ba2. (b) Detailed coordinates of the O atoms viewed from the [001] axis.

six kinds of O (O1–O6). As presented in Fig. 1a, spinel layers and conduction layers are alternately stacked together to form the BAO matrix with a  $\beta$ -Al<sub>2</sub>O<sub>3</sub> structure. In the conduction layer, the Al<sub>3</sub>/Al<sub>5</sub>–O tetrahedron constructs the structural frame, where Ba1 (CN = 9, Wyck. 2*d*) is accommodated in a large cavity formed by six Al<sub>5</sub>–O tetrahedra, while the spinel layer is called the “super structure layer” in the originally reported Ba- $\beta$ -Al<sub>2</sub>O<sub>3</sub> structure because of the unusual coordination environment.<sup>37</sup> As shown in the “Ba2 in spinel layer”, Ba2 and O3 are close to each other, and Al2 is wrapped by a Ba2–O polyhedron. According to the compiled atomic coordinates and occupancy information in Table S1,<sup>†</sup> the distance between Ba2 and O3 is calculated to be 0.342 Å, and the occupancy values of O3 and Ba2 are 0.957 and 0.043, respectively, suggesting that O3 and Ba2 atoms cannot exist at the same time. Correspondingly, Al2 with an occupancy of 0.957 is paired with O3 at the same time. The “spinel layer with Ba2” and “spinel layer without Ba2” are shown in the lower right part of Fig. 1(a). On one occasion, Ba2 (CN = 12) is coordinated with nine O1 and three O2 atoms and is tightly surrounded by the Al–O polyhedra. On another occasion, Al1, Al2 and Al4 are coordinated with O atoms to form the spinel layer.

The detailed coordination environments of O atoms in this structure are shown in Fig. 1b. Projecting from [001], there are three kinds of O-containing layers. Layers 1 and 3 are Ba-containing layers (Ba–O bond lengths are listed in Table S2<sup>†</sup>), in which O6 (Wyck. 6*h*) and O1 (Wyck. 12*k*) are coordinated with Ba1 and Ba2, respectively, while in layer 2, O2 (Wyck. 12*k*) acts as a linker between Ba1–O and Ba2–O polyhedra. O4 (Wyck. 4*e*) is separated from the Ba site.

Fig. 2a presents the XRD patterns of the synthesized BAON<sub>y</sub>:Eu samples ( $y = 0, 0.2, 0.4, 0.6, 0.8, 1.0$ ) as well as the standard pattern of BAO. The diffraction peaks of all the samples are in accordance with the standard card. For the synthesized BAO:Eu<sup>2+</sup> sample, the diffraction peaks shift to higher angles compared with the standard card, which can be attributed to the lattice shrinkage upon substitution of smaller Eu<sup>2+</sup> (1.3 Å, CN = 9) for Ba<sup>2+</sup> (1.47 Å, CN = 9).<sup>38</sup> Besides, as the enlarged XRD patterns presented in Fig. 2a reveal, the (–122) diffraction peak shifts to a lower angle, while the (017) diffrac-

tion peak shifts to a higher angle with increasing N<sup>3–</sup> concentration. This indicates an anisotropic change of the structure with the variation of composition.<sup>39</sup> The refined lattice parameters  $a$  and  $c$  as well as the cell volume ( $V$ ) are shown in Fig. 2b. It can be found that the lattice parameter  $a$  and  $V$  increase but  $c$  decreases, suggesting that N<sup>3–</sup> is more likely to occupy the lattice plane, which is abundant in O<sup>2–</sup> and perpendicular to the  $c$ -axis, as O1, O2, O4 and O6 crystallographic sites. However, the occupation of the N<sup>3–</sup> site cannot be verified accurately by XRD refinement owing to the similar weights of N<sup>3–</sup> and O<sup>2–</sup> ions; the detailed occupation of N<sup>3–</sup> sites will be discussed in combination with the spectral characterization later. Fig. S1<sup>†</sup> shows the Rietveld refinement results of BAON<sub>1.0</sub>:Eu, and the parameters of  $\chi^2$ ,  $R_{wp}$  and  $R_p$  are 3.11, 15.7% and 9.5%, respectively, establishing the reliability of this refinement. The detailed atomic coordinates and occupancy are listed in Table S3.<sup>†</sup>

Fig. S2a<sup>†</sup> presents the SEM image of BAON<sub>1.0</sub>:Eu. The microparticles are well crystallized to a hexagonal structure of around 15  $\mu$ m in size. The EDS elemental mappings in Fig. S2c–f<sup>†</sup> reveal that the constituent elements Eu, Ba, O and Al in the selected area (Fig. S2b<sup>†</sup>) present a uniform distribution. The color mapping of the N element in Fig. S2g<sup>†</sup> is not clear due to the low dopant. The N element concentration was further calculated to be 1.6 wt% using an element analysis instrument.

### 3.2. Luminescence properties

The PL spectra of BAON<sub>y</sub>:Eu phosphors under the excitation of 400 and 420 nm are presented in Fig. 3a and b. In Fig. 3a, at  $y = 0$ , the PL spectrum exhibits a broadband emission from 410 to 650 nm, which originates from the 5d → 4f transition of Eu<sup>2+</sup> in the BAO matrix. With increasing N<sup>3–</sup> concentration, the full width of half maximum (FWHM) values decreased from 141 to 68 nm (Fig. S3a<sup>†</sup>), accompanied by an obvious increase of the integrated PL intensity, and the integrated PL intensity at  $y = 1$  increases by about 1.7 times that at  $y = 0$ . Differing from the PL spectrum under 400 nm light excitation, the PL spectrum of BAO:Eu under 420 nm excitation shown in Fig. 3b reveals a distinct green emission peak at 518 nm with

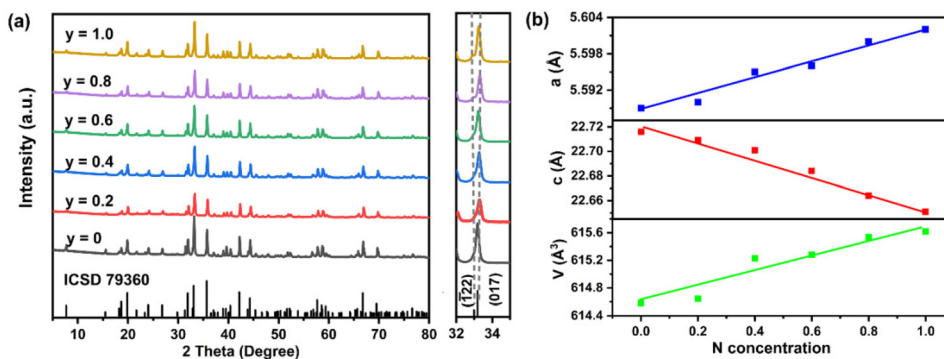
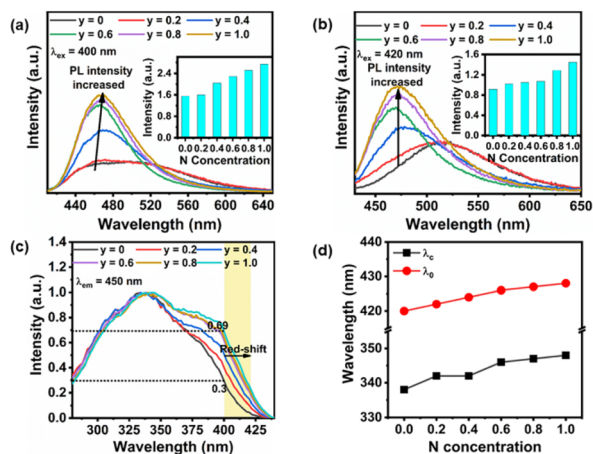


Fig. 2 (a) XRD patterns of BAON<sub>y</sub>:Eu ( $y = 0, 0.2, 0.4, 0.6, 0.8$  and  $1.0$ ) phosphors and the enlarged XRD patterns from 32–35 degrees. (b) Variation of the lattice parameters for BAON<sub>y</sub>:Eu phosphors.



**Fig. 3** PL spectra of  $\text{BAON}_y\text{:Eu}$  excited at (a) 400 and (b) 420 nm, respectively. The inset graphs show the corresponding integrated PL intensity variation with N concentration. (c) The normalized PLE spectra of  $\text{BAON}_y\text{:Eu}$  monitored at 450 nm. (d) The f-d spectroscopy parameters  $\lambda_0$  and  $\lambda_c$  of  $\text{BAON}_y\text{:Eu}$  phosphors based on the PLE spectra monitored at 450 nm.

FWHM value of 102 nm. This further indicates the two distinctive crystallographic sites of  $\text{Eu}^{2+}$  in BAO. In addition, with increasing  $\text{N}^{3-}$  concentration, the green emission submerges to background noise and PL bands are dominated by the blue emission when excited by both 400 and 420 nm, which may be owing to the redistribution of the  $\text{Eu}^{2+}$  ions in two kinds of Ba sites. However, it is difficult to distinguish the specific concentration of  $\text{Eu}^{2+}$  in these two kinds of Ba sites because the sheet-like morphology of the sample leads to a preferred orientation in the XRD measurements.

To figure out the reason for the PL intensity enhancement after nitridation, especially the blue emission, the normalized PLE spectra of  $\text{BAON}_y\text{:Eu}$  monitored at 450 nm were recorded and are depicted in Fig. 3c (the original PLE spectra are presented in Fig. S3b†). The broadband excitation ranging from the deep UV to violet region can be ascribed to the  $4f \rightarrow 5d$  transition of  $\text{Eu}^{2+}$ .<sup>40</sup> At  $y = 0$ , the excitation intensity at 400 nm is about 30% of that at the maximum. With increasing  $\text{N}^{3-}$  concentration, the PLE spectra shift to the long-wavelength region and the excitation intensity at 400 nm is enhanced to 69% of that at the maximum. The red-shifted PLE spectra indicate the samples are excited by violet light more efficiently, which is also beneficial for the application of violet-light-pumped phosphor-converted WLEDs.

Due to the naked 5d shell, the 5d energy level of  $\text{Eu}^{2+}$  is significantly subject to centroid shift and crystal field splitting. The f-d spectroscopy parameters of  $\text{Eu}^{2+}$  in  $\text{BAON}_y$  are depicted in Fig. 3d for comprehensively understanding the red-shift of the PLE spectra.  $\lambda_c$  refers to the centroid position of the excitation spectra, which is used the wavelength corresponding to half the integral intensity of the PLE spectrum.<sup>35</sup> The increased  $\lambda_c$  indicates that the partial nitridation strengthens the centroid shift, and this is ascribed to the higher covalency of  $\text{N}^{3-}$  than that of  $\text{O}^{2-}$ . Zero-phonon energy is deter-

mined by the crossing point of PL and PLE spectra, and the corresponding wavelength is marked as  $\lambda_0$ .<sup>41</sup> As a result,  $\lambda_0$  and  $\lambda_c$  present an identical tendency with increasing  $\text{N}^{3-}$  concentration, further suggesting that the doping of  $\text{N}^{3-}$  has little effect on the crystal field splitting but does on the centroid shift.<sup>42,43</sup>

### 3.3. Site selective occupation of $\text{N}^{3-}$

As shown in Fig. S3c,† different from that monitored at 450 nm, the PLE spectra of  $\text{BAON}_y\text{:Eu}$  monitored at 550 nm covers the range from the ultraviolet (UV) to the blue region, which further proves the multi-site occupation of  $\text{Eu}^{2+}$  ions. In addition, the normalized excitation spectra in Fig. S3d† are almost unchanged, indicating that the increasing substitution of  $\text{N}^{3-}$  has little effect on the centroid shift and crystal field splitting of long-wavelength emission. In order to determine the site selective occupation of  $\text{N}^{3-}$ , the PL spectrum of  $\text{BAO:Eu}$  was divided into two emission bands peaking at 2.45 and 2.77 eV through Gaussian deconvolution, as shown in Fig. 4a. According to the crystal field theory, a looser coordination environment corresponds to weaker crystal field splitting, and the polyhedra volumes centered at Ba1 and Ba2 are  $33.599 \text{ \AA}^3$  and  $50.83 \text{ \AA}^3$ , respectively.<sup>35,36</sup> Therefore, the emission bands peaking at 2.45 and 2.77 eV should be attributed to Eu in the Ba1 and Ba2 sites, respectively.

Fig. 4b shows the site selective occupation of  $\text{N}^{3-}$  on  $\text{O}^{2-}$ . According to the variation of lattice parameters in Fig. 1c, all the O1, O2, O4 and O6 crystallographic sites may be occupied by  $\text{N}^{3-}$ . Combined with the analysis of spectral properties, the incorporation of  $\text{N}^{3-}$  has little effect on the emission of Eu at the Ba1 site, which is coordinated with O2 and O6. Therefore, the possibility of  $\text{N}^{3-}$  occupying the O2 and O6 sites is very low, while Ba2 is coordinated with O1 and O2 and  $\text{N}^{3-}$  significantly affects the emission of Eu in the Ba2 site. Therefore, we think that  $\text{N}^{3-}$  selectively occupies the O1 site. Besides, given that O4 is far away from Ba1 and Ba2, the  $\text{N}^{3-}$  that occupies the O4 site does not exert a direct influence on the luminescence.

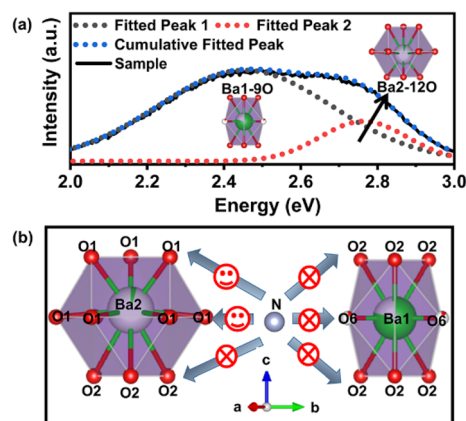


**Fig. 4** (a) Gaussian fitted PL spectrum of the  $\text{BAO:Eu}$  phosphor under the excitation of 400 nm violet light as well as the corresponding coordinated polyhedra. (b) Site selective occupation of  $\text{N}^{3-}$  on the O sites.

science properties, so the occupancy of  $N^{3-}$  on the O4 site remains unclear. We further tried to verify the lattice site occupation of  $N^{3-}$  by ND pattern calculations with  $N^{3-}$  substitution for the O1, O2, O4 and O6 sites, as depicted in Fig. S4a–d.† However, there is little difference of the simulation results between BAO:Eu and BAON<sub>1.0</sub>:Eu, indicating that the occupation of  $N^{3-}$  cannot be proved by ND effectively. In addition, negative defects may exist in the BAON<sub>y</sub>:Eu anionic solid solution due to the charge imbalance between  $O^{2-}$  and  $N^{3-}$  ions, and the positive oxygen vacancy defects may appear for charge compensation.

### 3.4. Luminescence thermal stability and quantum efficiency

The luminescence thermal stability of phosphors is an important criterion for evaluating their practical applications, since the working temperature of phosphor-converted WLEDs are up to 120 °C. Fig. 5a–c present the temperature-dependent PL spectra of BAON<sub>y</sub>:Eu ( $y = 0, 0.4$  and  $1.0$ ) phosphors in the temperature range of 80–500 K under the excitation of 400 nm. Correspondingly, the original PL spectra and color coordinates are given in Fig. S5.† As for the sample BAO:Eu, the slight redshift of emission peaks with increasing temperature can be ascribed to the energy transfer between two kinds of Eu lattice sites. As for the samples BAON<sub>0.4</sub>:Eu and BAON<sub>1.0</sub>:Eu, the PL peak positions are almost unchanged with increasing temperature, indicating better color stability after nitridation. Color coordinates in Fig. S5† are both little varied. Fig. 5d shows the correlation between the integrated emission intensity and the temperature of the abovementioned three samples. Benefiting from the rigid matrix, all these series of phosphors exhibit excellent thermal stability. At 423 K (150 °C), the integrated PL intensity at  $y = 0, 0.4$  and  $1.0$  are 91%, 96% and 95% of that at 300 K (room temperature), respectively. A 1% difference of thermal stability at  $y = 0.4$  and  $1.0$  may be caused by measurement errors, and the measurement results can only be

explained by the fact that the thermal stability of the nitrogenous samples is better than that of the non-nitrogenous samples. The configuration coordinate diagram in the inset of Fig. 5d can be used to explain the thermal quenching behavior of phosphors. Under violet light excitation, electrons transfer from the 4f ground state to the 5d excited state (1), and then return to the 4f ground state in the form of light emission (2). With increasing temperature, electrons may return to the 4f ground state in the form of non-radiative transitions because of thermal disturbance (processes (3) and (4)). Hence, the PL intensity decreases with increasing temperature.

In addition, as shown in Fig. S6,† under the excitation of 400 nm light, the IQE/EQE values of our synthesized BAO:Eu and BAON<sub>1.0</sub>:Eu phosphors are calculated to be 73%/32% and 80%/52%, respectively. This indicates the higher luminescence efficiency after nitridation. Table 1 lists the excitation/emission wavelengths, IQE/EQE values and thermal stability parameters of our BAON<sub>1.0</sub>:Eu phosphor and other reported blue phosphors, suggesting that BAON<sub>1.0</sub>:Eu can be an excellent candidate blue phosphor for full-spectrum WLED lighting.

### 3.5. Application

In order to verify the application of the blue BAON<sub>1.0</sub>:Eu phosphor, a WLED device was fabricated by combining a 405 nm violet chip with commercial (Sr, Ba)<sub>2</sub>SiO<sub>4</sub>:Eu, Sr<sub>3</sub>SiO<sub>5</sub>:Eu and CaAlSi<sub>3</sub>:Eu phosphors and our BAON<sub>1.0</sub>:Eu phosphor. Fig. 6a shows the WLED images with light on and off, as well as the corresponding color coordinates. The EL spectrum of the WLED at a driven current of 110 mA is shown in Fig. 6b, which presents a warm full-spectrum white light emission. The correlated color temperature (CCT) and  $R_a$  are calculated to be 3544 K and 95.4, respectively, and the luminous efficiency is 18.68 lm W<sup>-1</sup>. The special  $R_a$  values of R1–R15 all exceed 90 as shown in Fig. 6c. Besides, the normalized EL spectra at different currents of the WLED, shown in Fig. 6d, are almost unchanged without the obvious variation of intensity and peak position, indicating the excellent color stability of our packaged full-spectrum WLED for potential applications. In addition, an LED fabricated by combining a 405 nm violet chip with commercial (Sr, Ba)<sub>2</sub>SiO<sub>4</sub>:Eu, Sr<sub>3</sub>SiO<sub>5</sub>:Eu and CaAlSi<sub>3</sub>:Eu phosphors is presented in Fig. S7.† However, the color coordinates are not in the white light area because of the

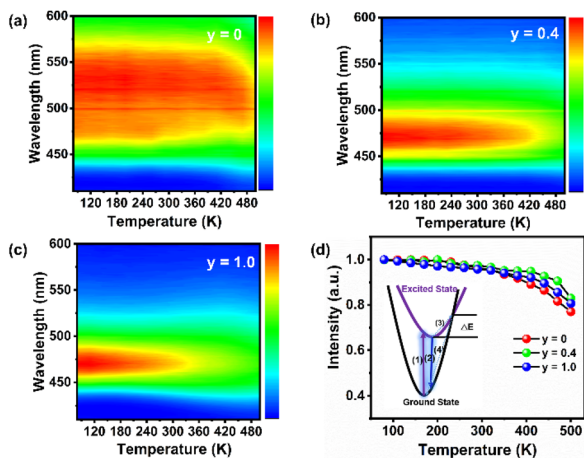
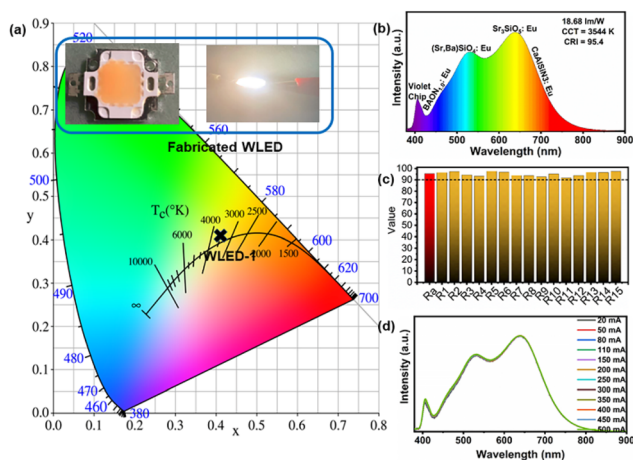


Fig. 5 Temperature-dependent PL spectra of BAON<sub>y</sub>:Eu phosphors at (a)  $y = 0$ , (b)  $0.4$  and (c)  $1.0$ . (d) Correlation between the integrated emission intensity and temperature; the inset shows the configuration coordinate diagram.

Table 1 Excitation/emission wavelengths, IQE/EQE values and thermal stability parameters of our BAON<sub>1.0</sub>:Eu phosphor and other reported blue phosphors

Phosphor	$\lambda_{ex}$ (nm)	$\lambda_{em}$ (nm)	IQE (%)	EQE (%)	$I_{150\text{ }^\circ\text{C}}/I_{RT}$	Ref.
BCM <sub>0.3</sub> S	400	475	82.9	66.2	90	6
(Na <sub>1.92</sub> Eu <sub>0.04</sub> )MgPO <sub>4</sub> F	400	456	71.9	<18.1	>100	9
K <sub>1.6</sub> Al <sub>11</sub> O <sub>17+δ</sub> :0.2Eu	400	450	92	39.7	>100	23
YScSi <sub>4</sub> N <sub>6</sub> C	400	469	30.3	—	48	44
Ca <sub>3</sub> Zr <sub>2</sub> SiGa <sub>2</sub> O <sub>12</sub> :Ce <sup>3+</sup>	400	478	42.7	—	48	45
Na <sub>3</sub> KMg <sub>7</sub> (PO <sub>4</sub> ) <sub>6</sub> :Eu	400	446	88	32.5	>100	46
BaHfSi <sub>3</sub> O <sub>9</sub> :Eu <sup>2+</sup>	405	475	50	39	86	47
BAON <sub>1.0</sub> :Eu	400	468	80	52	95	This work



**Fig. 6** (a) Color coordinates of the packaged WLED at the driven current of 110 mA. The inset images show the packaged WLED with its light on and off. (b) EL spectrum of the packaged WLED at a driven current of 110 mA. (c) The histogram of  $R_a$  and R1–R15 values of the WLED. (d) Normalized EL spectra of the WLED with different currents.

absence of a blue component, and the R12 value corresponding to the blue light is only 50, which is far from the standard of full-spectrum lighting. All these results demonstrate that the  $\text{BAON}_{1.0}\text{:Eu}$  phosphor has potential to be a blue light component in the fabrication of full-spectra WLEDs for high-quality lighting.

## 4. Conclusions

In this work, a series of blue  $\text{BAON}_y\text{:Eu}$  ( $y = 0, 0.2, 0.4, 0.6, 0.8, 1.0$ ) phosphors were synthesized by the high-temperature solid state method. With increasing substitution of  $\text{N}^{3-}$  for  $\text{O}^{2-}$ , the excitation spectra showed a continuous red-shift, and the PL spectra intensity increased at the excitation of violet light. Crystal structure, PL and PLE spectra analysis show that  $\text{N}^{3-}$  selectively occupies the O1 site and strengthens the 5d centroid shift of Eu in the Ba2 site, giving rise to a red-shift of the PLE spectrum. The IQE/EQE values of the optimal sample  $\text{BAON}_{1.0}\text{:Eu}$  excited by 400 nm violet light are 80%/52%, and the integrated emission intensity at 150 °C can remain at 95% of that at room temperature. Finally, a full-spectrum WLED device was fabricated by combining a violet chip with a blue  $\text{BAON}_{1.0}\text{:Eu}$  phosphor and other commercial phosphors. The  $R_a$  value is 95.4, and R1–R15 values all exceed 90. The results show that  $\text{BAON}_{1.0}\text{:Eu}$  excited by violet light is a promising blue phosphor candidate for full-spectrum WLED lighting, and this work also sheds light on the exploration of new phosphors.

## Conflicts of interest

There are no conflicts to declare.

## Acknowledgements

This work is supported by the National Natural Science Foundation of China (No. 51832005).

## References

- Z. Xia and Q. Liu, Progress in discovery and structural design of color conversion phosphors for LEDs, *Prog. Mater. Sci.*, 2016, **84**, 859–117.
- L. Wang, R.-J. Xie, T. Suehiro, T. Takeda and N. Hirosaki, Down-conversion nitride materials for solid state lighting: recent advances and perspectives, *Chem. Rev.*, 2018, **118**, 1951–2009.
- S. Li, Y. Xia, M. Amachraa, N. T. Hung, Z. Wang, S. P. Ong and R.-J. Xie, Data-driven discovery of full-visible-spectrum phosphor, *Chem. Mater.*, 2019, **31**, 6286–6294.
- X. Zhang, J. Zhang, X. Wu, L. Yu, Y. Liu, X. Xu and S. Lian, Discovery of blue-emitting  $\text{Eu}^{2+}$ -activated sodium aluminate phosphor with high thermal stability via phase segregation, *Chem. Eng. J.*, 2020, **388**, 124289.
- J. Oh, S. Yang and Y. Do, Healthy, natural, efficient and tunable lighting: four-package white LEDs for optimizing the circadian effect, color quality and vision performance, *Light: Sci. Appl.*, 2014, **3**, 314.
- S. Wang, Z. Song and Q. Liu, Recent progress in  $\text{Ce}^{3+}/\text{Eu}^{2+}$ -activated LEDs and persistent phosphors: focusing on the local structure and the electronic structure, *J. Mater. Chem. C*, 2023, **11**, 48–96.
- Y. Shao, H. Cai, F. Zhao, S. Liu, Z. Song and Q. Liu, Efficient violet-light-excitable blue-cyan phosphor for full-spectrum lighting, *Inorg. Chem. Front.*, 2022, **9**, 5590–5596.
- J. Zhong, Y. Zhuo, S. Hariyani, W. Zhao, J. Wen and J. Brgoch, Closing the cyan gap toward full-spectrum LED lighting with  $\text{NaMgBO}_3\text{:Ce}^{3+}$ , *Chem. Mater.*, 2020, **32**, 882–888.
- D. Wu, C. Shi, J. Zhou, Y. Gao, Y. Huang, J. Ding and Q. Wu, Full-visible-spectrum lighting enabled by site-selective occupation in the high efficient and thermal stable  $(\text{Rb}, \text{K})_2\text{CaPO}_4\text{F:Eu}^{2+}$  solid-solution phosphors, *Chem. Eng. J.*, 2022, **430**, 133062.
- S. Hariyani and J. Brgoch, Advancing human-centric LED lighting using  $\text{Na}_2\text{MgPO}_4\text{F:Eu}^{2+}$ , *ACS Appl. Mater. Interfaces*, 2021, **13**, 16669–16676.
- Z. Xu, B. Devakumar, N. Ma, W. Li and X. Huang, High-brightness cyan-emitting  $\text{Eu}^{2+}$ -activated orthophosphate phosphors for near-UV-pumped white LEDs, *J. Lumin.*, 2022, **243**, 118640.
- S. Huang, M. Shang, Y. Yan, Y. Wang, P. Dang and J. Lin, Ultra-broadband green-emitting phosphors without cyan gap based on double-heterovalent substitution strategy for full-spectrum WLED lighting, *Laser Photonics Rev.*, 2022, 2200473.
- Y. Yao, Z. Wang, Z. Yang, J. Cui, M. Zhang, X. Wang, M. Zheng, L. Cao, W. Ding and P. Li, A novel cyan-emitting

- phosphor  $\text{KScSrSi}_{2-y}\text{Ge}_y\text{O}_7:0.07\text{Bi}^{3+}$  for white LEDs with high color rendering index and low correlated color temperature, *CrystEngComm*, 2022, **24**, 2767.
- 14 R. E. Watson, N. K. Gibbs, C. E. Griffiths and M. J. Sherratt, Damage to skin extracellular matrix induced by UV exposure, *Antioxid. Redox Signal.*, 2014, **21**, 1063–1077.
  - 15 H. Chen, T. Seto and Y. Wang, An efficient blue phosphor with high thermal stability for lighting and optical pressure sensor applications, *Inorg. Chem. Front.*, 2022, **9**, 1644–1654.
  - 16 D. Böhnisch, J. Rosenboom, A. García-Fuente, *et al.*, On a blue emitting phosphor  $\text{Na}_3\text{RbMg}_7(\text{PO}_4)_6:\text{Eu}^{2+}$  showing ultrahigh thermal stability, *J. Mater. Chem. C*, 2019, **7**(20), 6012–6021.
  - 17 M. R. Krames, O. B. Shchekin, R. Mueller-Mach, *et al.*, Status and future of high-power light-emitting diodes for solid-state lighting, *J. Disp. Technol.*, 2007, **3**(2), 160–175.
  - 18 M.-H. Fang, Z. Bao, W.-T. Huang and R.-S. Liu, Evolutionary generation of phosphor materials and their progress in future applications for light-emitting diodes, *Chem. Rev.*, 2022, **122**, 11474–11513.
  - 19 J. S. Kim, Y. H. Park, S. M. Kim, J. C. Choi and H. L. Park, Temperature-dependent emission spectra of  $\text{M}_2\text{SiO}_4:\text{Eu}^{2+}$  (M = Ca, Sr, Ba) phosphors for green and greenish white LEDs, *Solid State Commun.*, 2005, **133**, 445–448.
  - 20 P. Li, Z. Yang, Z. Wang, Q. Guo and X. Li, Preparation and luminescence characteristics of  $\text{Sr}_3\text{SiO}_5:\text{Eu}^{2+}$  phosphor for white LED, *Chin. Sci. Bull.*, 2008, **53**, 974–977.
  - 21 X. W. Zhu, Y. Masubuchi, T. Motohashi and S. Kikkawa, The z value dependence of photoluminescence in  $\text{Eu}^{2+}$ -doped  $\beta\text{-SiAlON}$  ( $\text{Si}_{6-z}\text{Al}_2\text{O}_z\text{N}_{8-z}$ ) with  $1 \leq z \leq 4$ , *J. Alloys Compd.*, 2010, **489**, 157–161.
  - 22 H. Watanabe and N. Kijima, Crystal structure and luminescence properties of  $\text{Sr}_x\text{Ca}_{(1-x)}\text{AlSiN}_3:\text{Eu}^{2+}$  mixed nitride phosphors, *J. Alloys Compd.*, 2009, **475**, 434–439.
  - 23 V. Bachmann, C. Ronda, O. Oeckler, W. Schnick and A. Meijerink, Color Point Tuning for  $(\text{Sr,Ca,Ba})\text{Si}_2\text{O}_2\text{N}_2:\text{Eu}^{2+}$  for White Light LEDs, *Chem. Mater.*, 2009, **21**, 316–325.
  - 24 X. Qin, X. Liu, W. Huang, M. Bettinelli and X. Liu, Lanthanide-activated phosphors based on 4f–5d optical transitions: theoretical and experimental suspects, *Chem. Rev.*, 2017, **117**, 4488–4527.
  - 25 X. Li, P. Li, C. Liu, L. Zhang, D. Dai, Z. Xing, Z. Yang and Z. Wang, Tuning the luminescence of  $\text{Ca}_9\text{La}(\text{PO}_4)_7:\text{Eu}^{2+}$  via artificially inducing potential luminescence centers, *J. Mater. Chem. C*, 2019, **7**, 14601–14611.
  - 26 Y. Zhou, W. Zhuang, Y. Hu, R. Liu, H. Xu, M. Chen, Y. Liu, Y. Li, Y. Zheng and G. Chen, Cyan-green phosphor  $(\text{Lu}_2\text{M})(\text{Al}_4\text{Si})\text{O}_{12}:\text{Ce}^{3+}$  for high-quality LED lamp: tunable photoluminescence properties and enhanced thermal stability, *Inorg. Chem.*, 2019, **58**, 1492–1500.
  - 27 Z. Xia and A. Meijerink,  $\text{Ce}^{3+}$ -Doped garnet phosphors: composition modification, luminescence properties and applications, *Chem. Soc. Rev.*, 2017, **46**, 275–299.
  - 28 M. Liao, F. Wu, D. Zhu, X. Zhang, H. Dong, Z. Lin, M. Wen and Z. Mu, Towards single broadband white emission in  $\text{Rb}_{0.5}\text{K}_{1.5}\text{CaPO}_4(\text{F}, \text{Cl}):\text{Eu}^{2+}$  via selective site occupancy engineering for solid-state lighting applications, *Chem. Eng. J.*, 2022, **449**, 137801.
  - 29 Y. Wei, L. Cao, L. Lv, G. Li, J. Hao, J. Gao, C. Su, C. C. Lin, H. S. Jang, P. Dang and J. Lin, Highly efficient blue emission and superior thermal stability of  $\text{BaAl}_{12}\text{O}_{19}:\text{Eu}^{2+}$  phosphors based on highly symmetric crystal structure, *Chem. Mater.*, 2018, **30**, 2389–2399.
  - 30 X. Wu, R. Shi, J. Zhang, D. Wen, Z. Qiu, X. Zhang, W. Zhou, L. Yu and S. Lian, Highly efficient and zero-thermal-quenching blue-emitting  $\text{Eu}^{2+}$ -activated K-beta-alumina phosphors, *Chem. Eng. J.*, 2022, **429**, 132225.
  - 31 S. Piao, Y. Wang, X. Zhou, W. Geng, J. Zhang, X. Zhang, D. Wu, Y. Cao, X. Li and B. Chen, Defect engineering in a  $\text{Eu}^{2+}$ -doped  $\beta\text{-Al}_2\text{O}_3$  structure blue phosphor and its controllable zero-thermal quenching luminescence, *ACS Sustainable Chem. Eng.*, 2021, **9**, 7882–7890.
  - 32 K.-B. Kim, Y.-I. Kim, H.-G. Chun, T.-Y. Cho, J.-S. Jung and J.-G. Kang, Structural and optical properties of  $\text{BaMgAl}_{10}\text{O}_{17}:\text{Eu}^{2+}$  phosphor, *Chem. Mater.*, 2002, **14**, 5045–5052.
  - 33 S. Wang, Z. Song, Y. Kong, Z. Xia and Q. Liu, 5d-level centroid shift and coordination number of  $\text{Ce}^{3+}$  in nitride compounds, *J. Lumin.*, 2018, **200**, 35–42.
  - 34 P. Dorenbos, The 5d level positions of the trivalent lanthanides in inorganic compounds, *J. Lumin.*, 2000, **91**, 155–176.
  - 35 T. Wang, Z. Xia, Q. Xiang, S. Qin and Q. Liu, Relationship of 5d-level energies of  $\text{Ce}^{3+}$  with the structure and composition of nitride hosts, *J. Lumin.*, 2015, **166**, 106–110.
  - 36 G. Groppi, F. Assandri, M. Bellotto, C. Cristiani and P. Forzatti, The crystal structure of Ba- $\beta$ -alumina materials for high-temperature catalytic combustion, *J. Solid State Chem.*, 1995, **114**, 326–336.
  - 37 N. Iyi, Z. Inoue, S. Takekawa and S. Kimura, The crystal structure of barium lead hexaaluminate phase II, *J. Solid State Chem.*, 1985, **60**, 41–50.
  - 38 R. D. Shannon, Revised effective ionic radii and systematic studies of interatomic distances in halides and chalcogenides, *Acta Crystallogr.*, 1976, **32**, 751–767.
  - 39 L. He, Z. Song, X. Jia, Z. Xia and Q. Liu, Control of luminescence in  $\text{Eu}^{2+}$ -doped orthosilicate-orthophosphate phosphors by chainlike polyhedra and electronic structures, *Inorg. Chem.*, 2018, **57**, 609–616.
  - 40 W. Ji, S. Wang, Z. Song and Q. Liu, Luminescent thermal stability and electronic structure of narrow-band green-emitting  $\text{Sr-Sialon}:\text{Eu}^{2+}$  phosphors for LED/LCD backlights, *J. Alloys Compd.*, 2019, **805**, 1246–1253.
  - 41 T. Wang, Q. Xiang, Z. Xia, J. Chen and Q. Liu, Evolution of structure and photoluminescence by cation cosubstitution in  $\text{Eu}^{2+}$ -doped  $(\text{Ca}_{1-x}\text{Li}_x)(\text{Al}_{1-x}\text{Si}_{1+x})\text{N}_3$  solid solutions, *Inorg. Chem.*, 2016, **55**, 2929–2933.
  - 42 S. Wang, Z. Song, Y. Kong, Z. Xia and Q. Liu, Crystal field splitting of 4f<sub>n-1</sub>5d-levels of  $\text{Ce}^{3+}$  and  $\text{Eu}^{2+}$  in nitride compounds, *J. Lumin.*, 2018, **194**, 461–466.

- 43 P. Dorenbos, Crystal field splitting of lanthanide  $4f_{n-1}5d$ -levels in inorganic compounds, *J. Alloys Compd.*, 2002, **341**, 156–159.
- 44 C. Yan, Z. Liu, W. Zhuang, R. Liu, X. Xing, Y. Liu, G. Chen, Y. Li and X. Ma,  $\text{YScSi}_4\text{N}_6\text{C}:\text{Ce}^{3+}$ -A broad cyan-emitting phosphor to weaken the cyan cavity in full-spectrum white light-emitting diodes, *Inorg. Chem.*, 2017, **56**, 11087–11095.
- 45 J. Zhong, W. Zhuang, X. Xing, R. Liu, Y. Li, Y. Zheng, Y. Hu and H. Xu, Synthesis, structure and luminescence properties of new blue-green-emitting garnet-type  $\text{Ca}_3\text{Zr}_2\text{SiGa}_2\text{O}_{12}:\text{Ce}^{3+}$  phosphor for near-UV pumped white-LEDs, *RSC Adv.*, 2016, **6**, 2155–2161.
- 46 Z. Leng, H. Bai, Q. Qing, H. He, J. Hou, B. Li, Z. Tang, F. Song and H. Wu, A zero-thermal-quenching blue phosphor for sustainable and human-centric WLED lighting, *ACS Sustainable Chem. Eng.*, 2022, **10**, 10966–10977.
- 47 D.-Y. Wang, Y.-C. Wu and T.-M. Chen, Synthesis, crystal structure, and photoluminescence of a novel blue-green emitting phosphor:  $\text{BaHfSi}_3\text{O}_9:\text{Eu}^{2+}$ , *J. Mater. Chem.*, 2011, **21**, 18261–18265.